Chapter 31
A Frequency Shifter-Based Simple Control for Solar PV Grid-Interfaced System

Chinmay Jain and Bhim Singh

Abstract This paper deals with a grid-interfaced solar photovoltaic (SPV) energy conversion system for three-phase four-wire (3P4W) distribution system. The solar energy conversion system (SECS) is a multifunctional as it not only feeds SPV energy into the grid but also serves the purpose of grid current balancing, reactive power compensation, harmonic mitigation, and neutral current elimination. In a two-stage SPV system, the first stage is a boost converter, controlled with incremental conductance (InC) maximum power point tracking (MPPT) algorithm, and a second stage is a four-leg voltage source converter (VSC). A simple frequency shifter-based control is proposed for the control of VSC. A proportional integral (PI) controller along with feedforward term for SPV power is used for fast dynamic response. Simulations are carried out in MATLAB along with Simulink and Sim Power System toolboxes, and detailed simulation results are presented to demonstrate its required multifunctions.

31.1 Introduction

Vanishing conventional energy sources have moved world's attention toward non-conventional energy sources such as solar photovoltaic (SPV) and wind energy. The SPV systems are of prime interest because of low maintenance and no mechanical machine involvement in the energy conversion process. The solar PV systems can be

C. Jain (✉) · B. Singh
Department of Electrical Engineering, Indian Institute of Technology Delhi,
New Delhi 110016, India
e-mail: chinmay31jain@gmail.com

B. Singh
e-mail: bsingh@ee.iitd.ac.in

broadly classified into two categories, stand-alone and grid-interfaced systems [1]. The stand-alone PV systems are normally used at the places which are out of reach of the grid such as electric vehicle, satellites, and remote areas. The SPV is intermittent in nature; hence, the stand-alone system requires energy storage elements such as a battery to maintain instantaneous power balance between the load and the photovoltaic (PV) source. Three-port converters are proposed by researchers for power management between load, PV source, and batteries [2]. However, the use of batteries makes the system bulky and costly.

Grid-interfaced systems are becoming popular choice where the grid is available. In case of grid-interfaced system, the grid acts as infinitely large energy storage to take care of intermittency of PV source. Grid-interfaced PV inverters can be broadly classified into single-stage and two-stage systems. The single-stage system uses variable dc link voltage for maximum power point tracking (MPPT), and they usually inject currents at unity power factor (UPF) into the grid [3].

Some researchers have proposed reactive power compensation with the single-stage converter in the night time or cloudy days [4]. However, single-stage system is not effective in partial shedding conditions [5]. Dc link voltage rating is more in the case of single-stage grid-interfaced SPV system than in the case of two-stage system. In conventional two-stage system, the first stage extracts power from PV source and performs MPPT function, and the second stage feeds extracted energy into the grid. The main area of research in the grid-interfaced SPV system includes MPPT techniques, an increase in reliability and efficiency, a decrease in size, weight, and cost [6–10]. The reduction in cost can be achieved by two means, either directly or indirectly. The direct cost reduction includes reduction in installation cost or fixed cost, and in an indirect cost reduction, installation cost may be the same or a little higher, but the same resource is used efficiently so that the effective cost is reduced. The indirect cost reduction is an interesting area of research which includes allotting several other functions to the same resource which is being underutilized. In the case of grid-interfaced SPV system, the VSC for grid connection is underutilized when the power from solar PV array is less than its peak power at full irradiance. Hence, an indirect reduced cost system is proposed, which possesses several features other than feeding extracted energy at UPF.

The use of voltage source converter (VSC) as an active power filter is well known [11]. A fuzzy logic-based d–q axis current control is proposed in [12]. The synchronously rotating reference frame theory (SRFT)-based system requires tuning of phase-locked loop (PLL) and frame transformations. An instantaneous reactive power theory (IRPT)-based system is proposed in [13].The IRPT-based system operates on power-based calculation which suffers from poor dynamic response. Many researchers have proposed several soft computing theories for the control of VSC. Complicated adaptive and neural network-based control of VSC is also proposed in the literature which requires selection of optimal learning rate, tuning of internal parameters, and selection of hidden layers, and hence, these algorithms suffer from lack of intuition [14–17].

Nonlinear loads such as switched-mode power supplies (SMPS), electronic blasts, and microwave are increasing day by day. The increase in nonlinear loads is

causing severe power quality problems. In the case of nonlinear loads, the neutral conductor current is nonzero even in the case of balanced distribution of loads on three phases of the grid [18]. The neutral current increases losses in the system. In the case of unbalanced distribution of loads, the problem of neutral current becomes more severe and it may lead to bursting of neutral conductor in the case of an excessive neutral current. Several neutral current compensation techniques are reported in the literature, which include different transformer connections such as zigzag and star–delta [18, 19]. The use of a separate insulated gate bipolar transistor (IGBT) leg for neutral current compensation sharing common dc bus with 3-leg VSC is also reported in the literature [20].

In the proposed work, a three-phase, four-wire distribution system is considered for the study. A three-phase four-leg (3P4L) SECS is proposed, which not only performs the functions of grid interfacing but also possesses features such as harmonic mitigation, grid current balancing, neutral current elimination, and reactive power compensation. Adding extra features to the system helps in cost reduction of the system. A novel simple frequency shifter-based control is proposed for the control of VSC. The proposed control algorithm provides all the above-mentioned features to conventional 3P4L VSC topology. The control of the system has to perform MPPT and an active power filtering both at the same time. The proposed control algorithm is more suitable than a complicated control algorithm as it has very less number of calculations for extraction of fundamental component of load current in phase with phase voltage. The performance of the system is verified by means of MATLAB simulations. The presented system follows IEEE and IEC norms [21,22].

31.2 System Configuration

The proposed system configuration is shown in Fig. 31.1. A three-phase, four-wire distribution system is the system under consideration. The proposed system consists of a SPV array, a boost converter, a four-leg VSC, interfacing inductors, ripple filter, loads, and the grid. The system consists of SPV array, which is a series–parallel combination of small power solar panels to match the required rating. The solar array is interfaced with a dc–dc boost converter. The output of boost converter is connected to dc link of a four-leg VSC. The VSC acts as a controlled current source. The midpoints of VSC legs are connected to point of common coupling (PCC) via interfacing inductors. A ripple filter is connected in parallel at PCC to absorb switching ripple of VSC in PCC voltages. The loads to be compensated are also connected at PCC. The ratings of all the elements are given in Appendix.
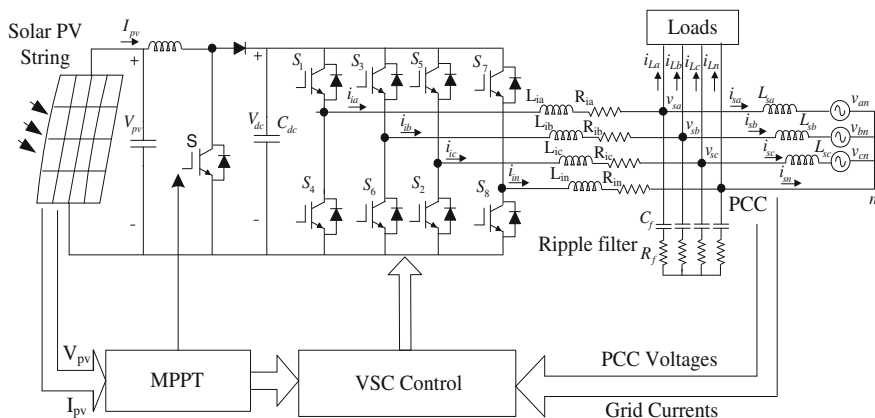
Fig. 31.1 System configuration

31.3 Control Algorithm

The control algorithm is the heart of the system. Figure 31.2 shows the proposed control algorithm. It decides the steady-state and dynamic behavior of the system. There are two main power circuits in the proposed system, i.e., the boost converter and the VSC. The output of the MPPT algorithm is the duty cycle for the boost converter. The VSC control decides the nature of injected current into the grid. Ideally, a grid-interfaced SPV system injects harmonic-free sinusoidal currents at UPF.

However, in the proposed system, the VSC provides compensation for harmonics, reactive power, neutral current, and load balancing. Hence, the currents injected by VSC are not to be sinusoidal, but the currents injected into the grid are to be sinusoidal. However, involving these extra features requires extra calculations in real time, and hence, a simple control is proposed incorporating comparatively low computations and meeting the grid norms. The two main portions of the control algorithm are as described in the following sections.

31.3.1 Maximum Power Point Tracking

An incremental conductance (InC)-based MPPT algorithm is used. The algorithm compares an InC with the conductance and takes the corrective action. The flow-chart for the algorithm is given in Fig. 31.2a. For calculation of InC, ΔI_{pv} and ΔV_{pv} are estimated as follows:

(a)

Read $V_{pv}(k)$, $I_{pv}(k)$

$\Delta V_{pv}=V_{pv}(k)-V_{pv}(k-1)$
$\Delta I_{pv}=I_{pv}(k)-I_{pv}(k-1)$

No ← $\Delta V_{pv}=0$ → Yes

$\Delta I_{pv}/\Delta V_{pv}=$ $-I_{pv}/V_{pv}$ Yes   Yes $\Delta I_{pv}=0$

No

$\Delta I_{pv}/\Delta V_{pv}>$ $-I_{pv}/V_{pv}$

Yes   No

$\Delta I_{pv}>0$
Yes   No

$V_{pv}\uparrow$ $V_{pv}\downarrow$

$V_{pv}\uparrow$ $V_{pv}\downarrow$

Update V_{pv}, $V_{pv}(k-1)$, I_{pv}, $I_{pv}(k-1)$

(b)
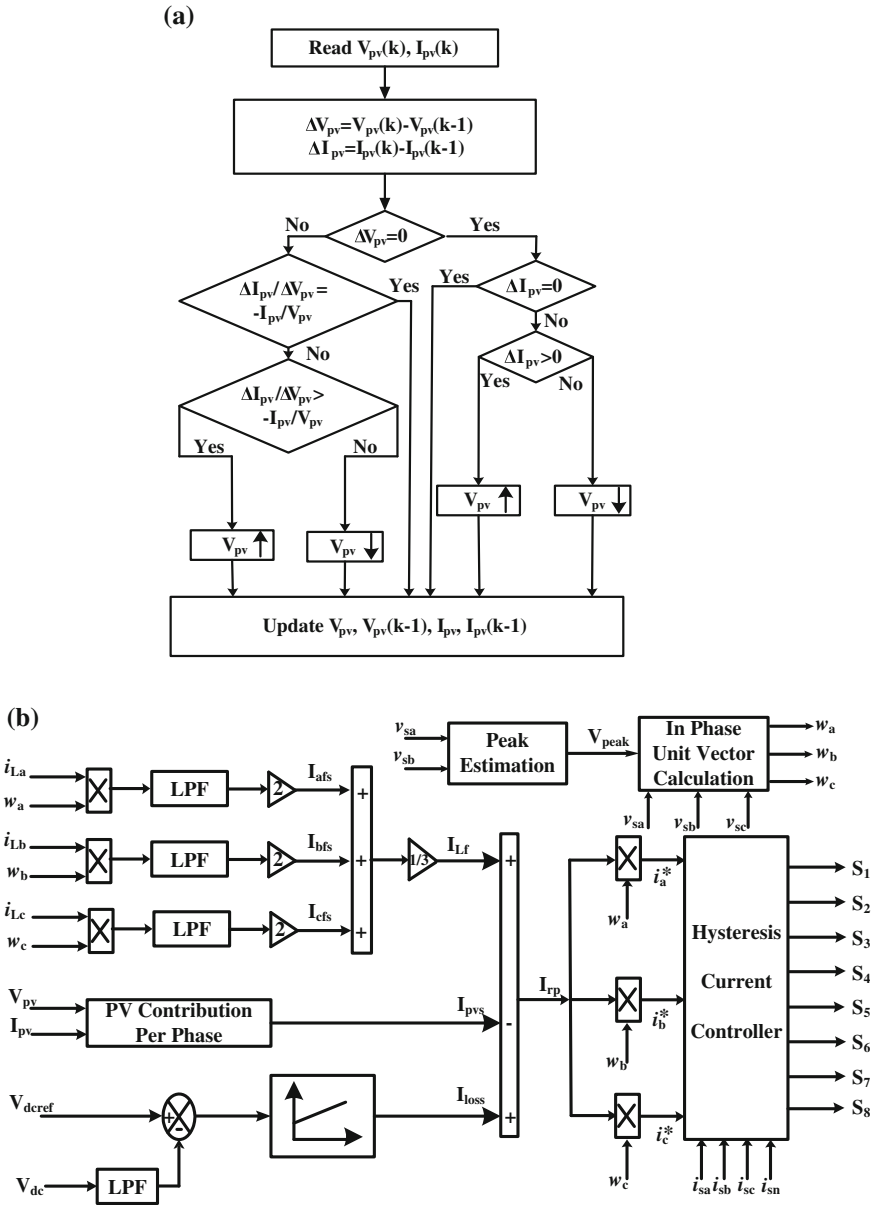
Fig. 31.2 **a** Flowchart for maximum power point tracking and **b** control strategy for VSC

$$\Delta I_{\text{pv}} = I_{\text{pv}}(k) - I_{\text{pv}}(k-1) \tag{31.1a}$$

$$\Delta V_{\text{pv}} = V_{\text{pv}}(k) - V_{\text{pv}}(k-1) \tag{31.1b}$$

where I_{pv} is the current from solar array and V_{pv} is the voltage across array.

The governing equations for MPPT algorithm are as follows:

$$\frac{\Delta I}{\Delta V} = \frac{-I}{V}, \text{ at MPP} \tag{31.2a}$$

$$\frac{\Delta I}{\Delta V} > \frac{-I}{V}, \text{ Left of MPP on } P_{\text{pv}}\text{v/s } V_{\text{pv}} \text{ curve} \tag{31.2b}$$

$$\frac{\Delta I}{\Delta V} < \frac{-I}{V}, \text{ Right of MPP on } P_{\text{pv}}\text{v/s } V_{\text{pv}} \text{ curve} \tag{31.2c}$$

31.3.2 Control Algorithm for Voltage Source Converter

For the control of VSC, two-phase PCC voltages (v_{sa}, v_{sb}), three-phase grid currents (i_{sa}, i_{sb}, i_{sc}), three-phase load currents (i_{La}, i_{Lb}, i_{Lc}), dc link voltage (V_{dc}), PV voltage (v_{pv}), and PV current (I_{pv}) are sensed. A feedforward term to accommodate changes in solar power is added in the control algorithm for fast dynamic response. The basic block diagram of control algorithm is given in Fig. 31.2b.

The sensed PCC voltages are passed through a band-pass filter to eliminate switching ripples. The peak is detected by the equation:

$$V_{\text{peak}} = \sqrt{\frac{2(v_{\text{sa}}^2 + v_{\text{sb}}^2 + v_{\text{sc}}^2)}{3}} \tag{31.3}$$

From peak, the in-phase unit vectors can be determined as follows:

$$w_a = \frac{v_{\text{sa}}}{V_{\text{peak}}}, \quad w_b = \frac{v_{\text{sb}}}{V_{\text{peak}}}, \quad w_c = \frac{v_{\text{sc}}}{V_{\text{peak}}} \tag{31.4}$$

The total power from SPV array is distributed equally to all the phases. The per phase contribution from solar PV can be calculated as follows:

$$I_{\text{pvs}} = \frac{2 \times P_{\text{pv}}}{3 \times V_{\text{peak}}} \tag{31.5}$$

The load current is multiplied with the corresponding in-phase unit templates, and the output of multiplication is then passed through a low-pass filter (LPF). The output of LPF is passed through a gain of two, and the net signal is termed as

magnitude of the load current in phase with the grid voltage. The mathematical background behind this control for phase a can be described as follows:

$$i_{La} = i_{fa} + \Sigma i_{ha} \tag{31.6}$$

where i_{fa} fundamental component of phase a load current which can be rewritten as

$$i_{fa} = I_{fas} \sin \omega_0 t + I_{fac} \cos \omega_0 t \tag{31.7a}$$

$$i_{La} \times \sin \omega_0 t = (I_{fas} \sin^2 \omega_0 t + I_{fac} \cos \omega_0 t \times \sin \omega_0 t) + \Sigma i_{ha} \times \sin \omega_0 t \tag{31.7b}$$

$$i_{La} \times \sin \omega_0 t = \frac{I_{fas}}{2} + \left(\frac{I_{fac}}{2} \sin 2\omega_0 t - \frac{I_{fas}}{2} \cos 2\omega_0 t \right) + \Sigma i_{ha} \times \sin \omega_0 t \tag{31.7c}$$

From Eq. (31.7c), it can be concluded that the frequency of fundamental current is shifted to double-harmonic frequency and dc frequency, out of which in-phase fundamental component is shifted to 0 Hz with a scaling factor of half. All other harmonic components and quadrature of fundamental are shifted to second or higher order. Shifting the in-phase component to 0 Hz gives benefit of zero phase shifts in reference currents in steady-state condition. Similarly, in-phase component of fundamental current can be determined for phase b and phase c. All in-phase components of load currents are added, and the net addition gives total active component of load currents. The output of addition is divided by 3 to distribute load fundamental active power component of current equally to all the phases, which gives average per phase active power component of load current (I_{Lf}).

The output of PI controller is added to I_{Lf}. The SPV contribution per phase (I_{pvs}) is subtracted from the load current and loss component which gives net active power component for the grid (I_{rp}). The I_{rp} is then multiplied with unit templates to get the reference grid currents for three phases, and reference current for neutral leg is set zero.

The sensed and reference currents are given as the inputs to hysteresis current controller, and logic switching pulses are output of the current controller.

31.4 Result and Discussion

The proposed two-stage grid-interfaced SPV system is modeled in MATLAB along with Simulink and Sim Power System toolboxes. A SPV array rating of 25 kW is considered, and a load power rating of 5 kW per phase is considered. The performance of the system is verified via simulations. Simulation results for the system are presented and discussed under various loading conditions of the grid. Simulation results are presented for linear, nonlinear, and change in insolation levels. The harmonic analysis of the load and grid currents is also presented to demonstrate harmonic mitigation capability of the proposed system. The system parameters used for simulation study are given in Appendix.

31.4.1 Performance of System Under Linear Load

The performance of the proposed system under linear load condition is shown in Fig. 31.3a. At time $t = 0.3$ s, the system is working under power factor correction mode. At time $t = 0.35$ s, phase c load is opened, and at time $t = 0.4$ s, phase a load is opened. The load currents are unbalanced to demonstrate dynamic behavior of the system. It can be observed that load currents are unbalanced, but grid currents are balanced sinusoids at UPF. As the load is unbalanced, the neutral current can be observed in load neural (i_{Ln}). The VSC neutral current (i_{VSCn}) is equal and opposite to load neural current. The grid neutral current (i_{sn}) is compensated to zero. When the load is thrown, the load power decreases, and at the same time, if PV power is kept constant, then the power injected into the grid increases. The increment in power injected into the grid can be observed in the form of increment in grid currents. When the load is added again, the decrement in grid currents can be observed. During unbalancing, no appreciable effect is observed on dc link voltage (V_{dc}) and power from solar PV array (P_{pv}).

31.4.2 Performance of System Under Nonlinear Load

Figure 31.3b shows the performance of the proposed system under nonlinear load. A nonlinear load of 5 kW is considered on each phase. The power from solar PV array is considered to be constant. At $t = 0.3$ s, the grid currents are balanced and sinusoidal at UPF. The VSC is supplying all the harmonic currents required. For nonlinear loads, neural currents can be observed even for balanced load. The load neutral current increases in the case of unbalanced loading of the system. The load and VSC neutral currents are out of phase which results in zero current in grid neutral conductor. Phase c load is removed at $t = 0.35$ s and added at $t = 0.45$ s, respectively. Similarly, load on phase a is also varied. It can be observed that grid currents are balanced and sinusoidal even in the case of unbalanced nonlinear load on the system. The VSC currents are unbalanced to make grid currents balance sinusoids. When the load power is decreased, an increase in grid currents is observed on account of an increase in injected power into the grid. During load unbalancing, no appreciable effect is observed on dc link voltage (V_{dc}) and power from solar PV array (P_{pv}).

31.4.3 Performance of System for Step Change in Irradiance

Performance of the system for step change in irradiance is shown in Fig. 31.3c. At $t = 0.4$ s, the irradiance is 1,000 W/m^2. The load on the system is unchanged which can be observed from load currents. The power from the solar PV array is 25 kW,

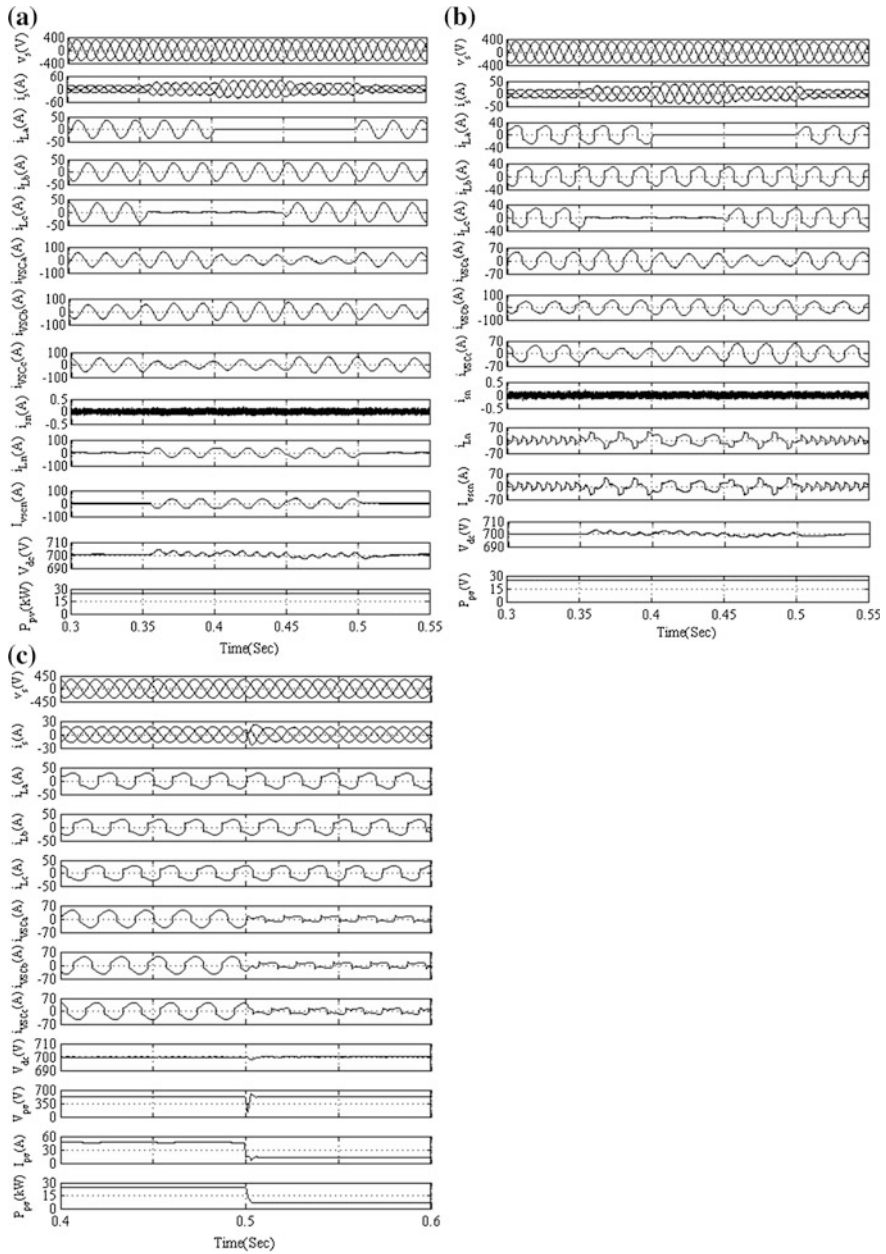**Fig. 31.3 a** Behavior of system for linear load, **b** behavior of system for nonlinear load, and **c** behavior of system for step change in insolation
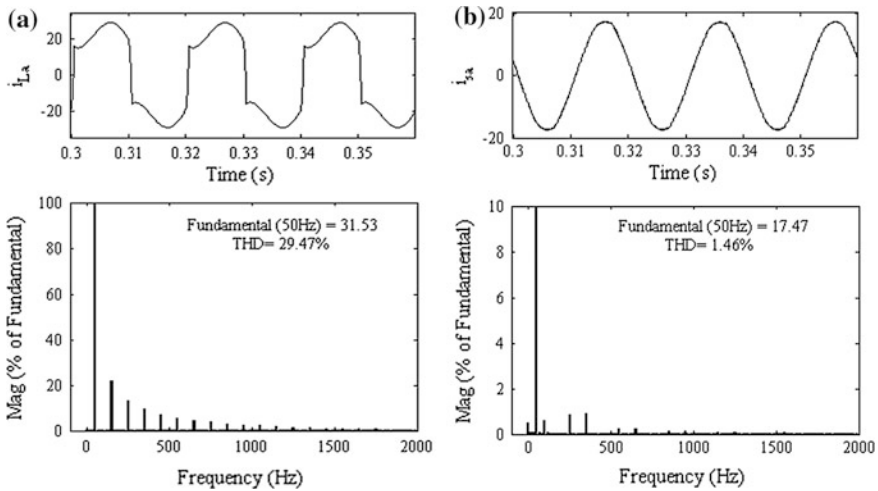
Fig. 31.4 **a** Load current and its THD and **b** grid current and its THD

and the load power is 15 kW; hence, the difference power is being fed into grid. The VSC currents consist of harmonic currents and fundamental currents corresponding to active power from solar PV array. At time $t = 0.5$ s, the irradiance is changed to 300 W/m^2. The decrease in irradiance causes a decrease in power from SPV array. It can be easily observed that solar PV power (P_{pv}) is less than the load power after a decrease in irradiance.

The reversal in the phase of grid currents can be seen, which shows that after $t = 0.5$ s, the real power is drawn from the grid. The grid currents are balanced and harmonic free.

31.4.4 Harmonic Analysis

Figure 31.4 shows the harmonic analysis of load and grid currents. Figure 31.4a shows the load current and harmonic analysis for load current. Figure 31.4b shows grid current and harmonic analysis of grid current. It can be observed that the total harmonic distortion (THD) of load current is 29.47 %, whereas THD of grid current is 1.46 %. The THD of grid current is well under 5 % limit of IEEE-519 standard.

31.5 Conclusion

A two-stage, three-phase, four-leg VSC-based system has been proposed to interface solar PV array with a 3P4W distribution system. A simple control with reduced calculations has been proposed to interface SPV to the grid. The proposed control

algorithm had been found fast, accurate, and easy for real-time implementation. A simple control has selected as VSC in the proposed topology which serves not only the functions of power quality improvement at the grid but also neutral current compensation and interfacing SPV with the grid. The proposed interfacing SPV array in the distribution system reduces losses in the power system, and multi-functionality of VSC improves the utilization factor of VSC. The simplicity of frequency shifter algorithm makes feasible and easy implementation of proposed multifunctional VSC. The performance of proposed control has been demonstrated under different loading and weather conditions. Both dynamic and steady-state performances have been found satisfactory. The THD of grid current meets IEEE and IEC standards.

Appendix

SPV Data: panel short-circuit current (I_{scn}) = 8.2 A, panel open-circuit voltage (V_{ocn}) = 32.8 V, panel current at MPP (I_{mpp} at 1,000 W/m^2) = 7.59 A, panel voltage at MPP (V_{mpp} at 1,000 W/m^2) = 27.89 V, voltage temperature coefficient (K_v) = −82e−3 V/K, current temperature coefficient (K_i) = 0.0031 A/K, number of series cell in each panel = 54, number of panels in series = 21, and number of panels in parallel = 6. Supply system parameters: supply voltage rms line to line 415 V, frequency = 50 Hz, grid source inductance = 3 mH/phase, grid source resistance = 0.312 Ω/phase, ripple filter R = 5 Ω, C = 5 μF, K_{ploss} = 1, K_{iloss} = 0.1.

References

1. Wang Z, Fan S, Zheng Y, Cheng M (2012) Control of a six-switch inverter based single-phase grid-connected PV generation system with inverse park transform PLL. In: Proceedings of international symposium on industrial electronics (ISIE), pp 258–263
2. Chen Y, Wen G, Peng L, Kang Y, Chen J (2013) A family of cost-efficient non-isolated single-inductor three-port converters for low power stand-alone renewable power applications. In: Proceedings of twenty-eighth annual IEEE applied power electronics conference and exposition (APEC), pp 1083–1088
3. Chen Y, Smedley KM (2004) A cost-effective single-stage inverter with maximum power point tracking. IEEE Trans Power Electron 19(5):1289–1294
4. Libo W, Zhengming Z, Jianzheng L (2007) A single-stage three-phase grid-connected photovoltaic system with modified MPPT method and reactive power compensation. IEEE Trans Energy Convers 22(4):881–886
5. Kashif MF, Choi S, Park Y, Sul SK (2012) Maximum power point tracking for single stage grid-connected PV system under partial shading conditions. In: Proceedings of 7th international power electronics and motion control conference (IPEMC), vol. 2, pp 1377–1383

6. Koutroulis E, Blaabjerg F (2013) Design optimization of transformerless grid-connected PV inverters including reliability. IEEE Trans Power Electron 28(1):325–335
7. Shimizu T, Suzuki S (2011) Control of a high-efficiency PV inverter with power decoupling function. In: Proceedings of 8th international conference on power electronics and ECCE Asia (ICPE & ECCE), pp 1533–1539
8. Liang Z, Guo R, Li J, Huang A (2011) A high-efficiency PV module-integrated DC/DC converter for PV energy harvest in FREEDM systems. IEEE Trans Power Electron 26 (3):897–909
9. Gu Y, Li W, Zhao Y, Yang B, Li C, He X (2013) Transformerless inverter with virtual DC bus concept for cost-effective grid-connected PV power systems. IEEE Trans Power Electron 28 (2):793–805
10. Hendriks JW, Fransen HPW, Van Zolingen RJC (1995) Reliable cost effective photovoltaic (PV) systems system approach with one-source responsibility. In: Proceedings of 17th international conference on telecommunications energy, pp 755–757
11. Emadi A, Nasiri A, Bekiarov SB (2005) Uninterruptible power supplies and active filters. CRC Press, New York
12. Yatak MO, Bay OF (2011) Fuzzy control of a grid connected three phase two stage photovoltaic system. In: Proceedings of international conference on power engineering, energy and electrical drives (POWERENG), pp 1–6
13. Singh B, Solanki J (2009) A comparison of control algorithms for DSTATCOM. IEEE Trans Industr Electron 56(7):2738–2745
14. Kumar P, Mahajan A (2009) Soft computing techniques for the control of an active power filter. IEEE Trans Power Delivery 24(1):452–461
15. Han Y, Xu L, Khan MM, Chen C, Yao G, Zhou LD (2011) Robust deadbeat control scheme for a hybrid APF with resetting filter and ADALINE-based harmonic estimation algorithm. IEEE Trans Industr Electron 58(9):3893–3904
16. Hammoudi MY, Allag A, Mimoune SM, Ayad M-Y, Becherif M, Miraoui A (2006) Adaptive nonlinear control applied to a three phase shunt active power filter. In: Proceedings of IEEE international conference on industrial technology, pp 762–767
17. Lam CS, Choi WH, Wong MC, Han YD (2012) Adaptive DC-link voltage controlled hybrid active power filters for reactive power compensation. IEEE Trans Power Electron 27 (4):1758–1772
18. Negi A, Surendhar S, Kumar SR, Raja P (2012) Assessment and comparison of different neutral current compensation techniques in three-phase four-wire distribution system. In: Proceedings of 3rd IEEE international symposium on power electronics for distributed generation systems, pp 423–430
19. Singh B, Jayaprakash P, Kothari DP (2010) Magnetics for neutral current compensation in three-phase four-wire distribution system. In: Proceedings of joint international conference on power electronics, drives and energy systems (PEDES) and power India, pp 1–7
20. Srikanthan S, Mishra MK (2010) Modeling of a four-leg inverter based DSTATCOM for load compensation. In: Proceedings of international conference on power system technology (POWERCON) pp 1–6
21. IEEE Recommended Practices and Requirement for Harmonic Control on Electric Power System, IEEE Std. 519 (1992)
22. Limits For Harmonic Current Emissions, International Electrotechnical Commission IEC-61000-3-2 (2000)